RADC-TR-76-379
IN-HOUSE REPORT
DECEMBER 1976

Effect of Multipath on the Height-Finding Capabilities of a Fixed-Reflector Radar System

Part 3: Effect of Radome

RONALD L. FANTE
PETER R. FRANCHI
RICHARD L. TAYLOR

ROME AIR DEVELOPMENT CENTER
AIR FORCE SYSTEMS COMMAND
GRIFFISS AIR FORCE BASE, NEW YORK 13441

This report has been reviewed by the RADC Information Office (O) and is releasable to the National Technical Service (NTIS). At NTIS it will be releasable to the general public, including foreign nations.

This technical report has been reviewed and approved for publication.

APPROVED:

WALTER ROTMAN, Chief
Microwave Detection Techniques Branch

APPROVED:

ALLAN C. SCHELL
Acting Chief
Electromagnetic Sciences Division

FOR THE COMMANDER:

Plans Office

Unclassified

SECURITY CLASSIFICATION OF THIS PAGE (When Data Entered)

REPORT DOCUMENTATION PAGE

READ INSTRUCTIONS BEFORE COMPLETING FORM

1. REPORT NUMBER: RADC-TR-76-379	2. GOVT ACCESSION NO. / 3. RECIPIENT'S CATALOG NUMBER
4. TITLE (and Subtitle): EFFECT OF MULTIPATH ON THE HEIGHT-FINDING CAPABILITIES OF A FIXED-REFLECTOR RADAR SYSTEM, Part 3: Effect of Radome	5. TYPE OF REPORT & PERIOD COVERED: In-house
	6. PERFORMING ORG. REPORT NUMBER
7. AUTHOR(s): Ronald L. Fante, Peter R. Franchi, Richard L. Taylor	8. CONTRACT OR GRANT NUMBER(s)
9. PERFORMING ORGANIZATION NAME AND ADDRESS: Deputy for Electronic Technology (RADC/ETEP), Hanscom AFB, Massachusetts 01731	10. PROGRAM ELEMENT, PROJECT, TASK AREA & WORK UNIT NUMBERS: 62702F, 2305J401
11. CONTROLLING OFFICE NAME AND ADDRESS: Deputy for Electronic Technology (RADC/ETEP), Hanscom AFB, Massachusetts 01731	12. REPORT DATE: Dec[redacted]76
	13. NUMBER OF PAGES: 15
14. MONITORING AGENCY NAME & ADDRESS (if different from Controlling Office)	15. SECURITY CLASS. (of this report): Unclassified
	15a. DECLASSIFICATION/DOWNGRADING SCHEDULE

16. DISTRIBUTION STATEMENT (of this Report)

Approved for public release. Distribution unlimited.

17. DISTRIBUTION STATEMENT (of the abstract entered in Block 20, if different from Report)

18. SUPPLEMENTARY NOTES

19. KEY WORDS (Continue on reverse side if necessary and identify by block number)

Radar
Reflector antennas
Radomes

20. ABSTRACT (Continue on reverse side if necessary and identify by block number)

It has been demonstrated that the ribs of the CW-396A radome have a negligible effect on the L-band elevation plane radiation pattern and consequently on the altitude error curves for the air-search radar discussed in Part 2 of this report (RADC-TR-76-215). In particular, the radome produces grating lobes that are approximately 30 dB below the main beam level.

DD FORM 1473, 1 JAN 73 — EDITION OF 1 NOV 65 IS OBSOLETE

Unclassified

SECURITY CLASSIFICATION OF THIS PAGE (When Data Entered)

SECURITY CLASSIFICATION OF THIS PAGE(*When Data Entered*)

SECURITY CLASSIFICATION OF THIS PAGE(When Data Entered)

Contents

Illustrations

Tables

Effect of Multipath on the Height-Finding Capabilities of a Fixed-Reflector Radar System

Part 3: Effect of Radome

1. INTRODUCTION

In Parts 1 and 2 of this report we studied the effect of multipath on the height-finding capabilities of an air-search radar. In this portion, we will consider the effects of a radome on the radiation pattern.

We showed previously that, in the absence of any radome or multipath, the magnetic field in the Fraunhofer zone of an arbitrary reflector can be written as

$$H_s = \frac{-jk}{2\pi R_o} \iint_{s_o} dx\, dy \left[\left(\hat{z} - \hat{x}\frac{\partial f}{\partial x} - \hat{y}\frac{\partial f}{\partial y} \right) \times \underline{H}_i \right]$$

$$\times \left[\hat{x} \sin\theta \cos\phi + \hat{y} \sin\theta \sin\phi + \hat{z} \cos\theta \right] \exp(-jkR) \ , \qquad (1)$$

where the reflector surface satisfies the equation $z = f(x, y)$, $\underline{H}_i$ is the field incident on the reflector from the feed horn, and s_o the projection of the reflector on the x-y plane. The quantities R_o, R, θ and ϕ are shown on Figure 1.

Now let us suppose that the reflector is placed inside a CW-396A radome. It has been demonstrated elsewhere[1] that, for this type of radome, only the radome

(Received for publication 10 Dec 1976)

1. Blank, C. M. (1961) Effects of CW-396A Radome on AN FPS-6 Performance, Rome Air Development Center Report RADC-TN-61-189.

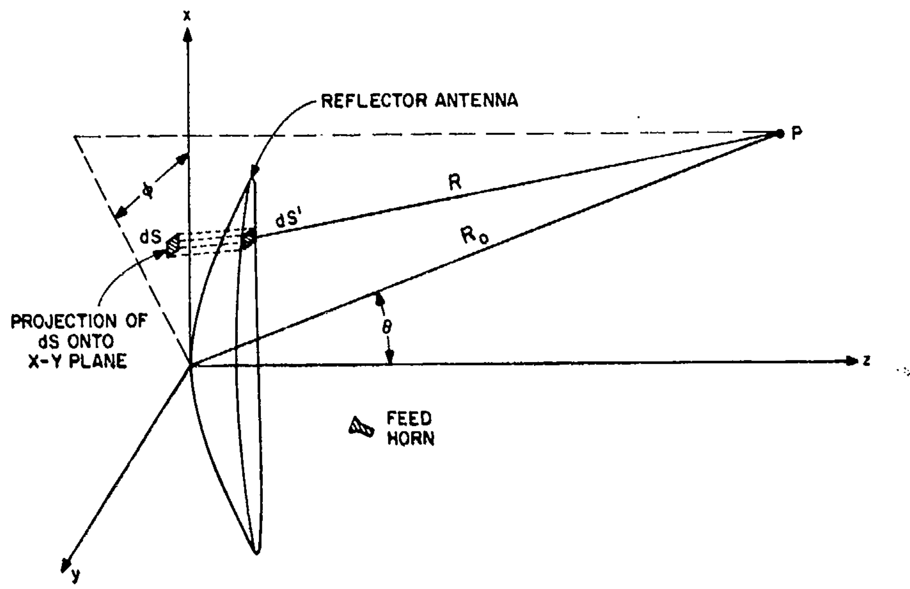

Figure 1. Assumed Reflector Geometry. Note that ϕ lies in the x-y plane

ribs significantly influence the radiation pattern, and the effect of the radome panels and bolts can be neglected. For purposes of calculation, we have found it convenient to approximate the rib structure by one which is periodic, as shown in Figure 2. The coordinates ψ and η are defined in Figure 3.

In order to calculate the effect of the radome on the radiation field we employ the equivalent current method.[2] In this method, we calculate the field scattered by each radome rib and then approximate that rib by a current sheet which produces the same radiation field. This current sheet is then projected back onto the reflector, so that the net reflector surface current is the original surface current plus the surface currents due to all the radome ribs projected onto the aperture. Therefore, in place of Eq. (1) we get

$$H_s = \frac{-jk}{2\pi R_o} \iint_{S_o} dx\, dy \left[\left(\hat{z} - \hat{x}\frac{\partial f}{\partial x} - \hat{y}\frac{\partial f}{\partial y}\right) \times \underline{H}_i \right] (1 + K(x,y) \exp(jkh \cos\theta))$$

$$\times \; [\hat{x} \sin\theta \cos\phi + \hat{y} \sin\theta \sin\phi + \hat{z} \cos\theta] \exp(-jkR) \quad , \qquad (2)$$

2. Kennedy, P. D. (1958) An Analysis of the Electrical Characteristics of Structurally Supported Radomes, Ohio State University, Antenna Laboratory Report 722-8.

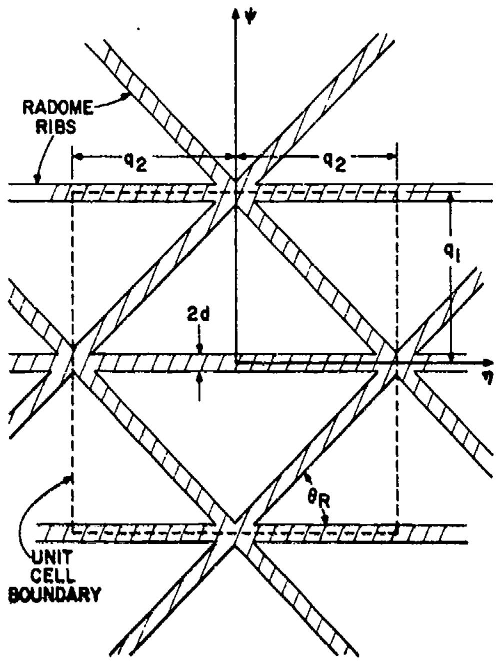

Figure 2. Radome Structure

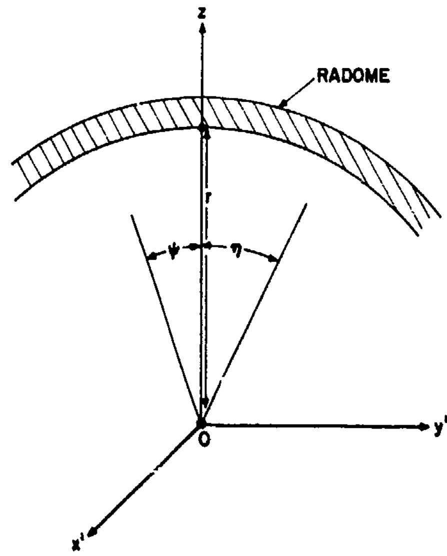

Figure 3. Radome Geometry. Note that ψ lies in the x'-z plane and η lies in the y'-z plane

where K(x, y) is the (complex) equivalent surface current which yields the same far field as the scattering by the radome rib and kh cos θ is the phase correction between the actual location of the radome ribs and their equivalent projection on the aperture surface. If the radome radius is denoted by r and x_2, y_2, z_2 are the coordinates of the center of the reflector in the coordinate system of Figure 3, we can easily show that

$$h = [r^2 - (x + x_2)^2 - (y + y_2)^2]^{1/2} - (z + z_2) \quad . \tag{3}$$

In the next section, we will discuss the calculation of the equivalent current density K.

2. CALCULATION OF THE EQUIVALENT RIB CURRENT

Let us consider a radome rib and assume that (due to the reflector) there is some field $\underline{E}$ incident upon it, which we can decompose onto components $E^{\parallel}$ and $E^{\perp}$ which are respectively parallel and transverse to the long dimension of the rib, as shown in Figure 4. The long dimension of the rib is normal to the paper (Figure 4) and we have chosen the coordinate system (u, v) so that the v axis lies along the direction of propagation of the incident wave. We should like to solve for the electric field scattered by this rib, for mathematical convenience we shall use the approximation that the rib is infinitely long in the direction normal to the paper. In order to solve for the scattered field, we must first obtain the field inside the rib; if we divide the rib into N small cells as shown in Figure 4, it can be shown that the field $\underline{e}$ at the center of each cell satisfies[3]

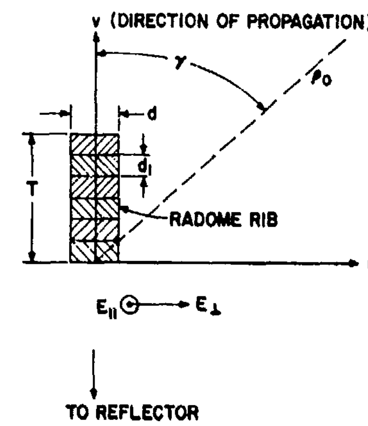

Figure 4. Geometry Assumed for Calculating the Scattering by the Radome Ribs

$$\sum_{n=1}^{N} C_{mn} e_n^{\parallel} = E_m^{\parallel} \qquad m = 1, 2, 3 \ldots N , \tag{4}$$

$$\sum_{n=1}^{N} A_{mn} e_n^{\perp} = E_m^{\perp} \qquad m = 1, 2, 3 \ldots N , \tag{5}$$

where

$$C_{mm} = 1 + \frac{1}{2} (\epsilon - 1) [\pi ka \, H_1^{(2)} (ka) - 2j] ,$$

$$C_{mn} = j \frac{\pi ka}{2} (\epsilon - 1) J_1 (ka) \, H_0^{(2)} (k\rho_{mn}) ,$$

$$A_{mm} = 1 + (\epsilon - 1) [j \frac{\pi ka}{4} H_1^{(2)} (ka) + 1] ,$$

$$A_{mn} = \frac{j\pi a (\epsilon - 1) J_1 (ka)}{2\rho_{mn}} [k\rho_{mn} H_0^{(2)} (k\rho_{mn}) - H_1^{(2)} (k\rho_{mn})] ,$$

ϵ = relative permittivity of the rib,

$\rho_{mn} = | m - n | d_1$

3. Richmond, J.H. (1966) Scattering by a dielectric cylinder of arbitrary cross section shape, IEEE Tr. AP AP-14:334-341;460-464.

$a = (d_1 d/\pi)^{1/2}$, and

$H_0^{(2)}$ = Hankel function of the second kind.

If we assume that the incident field propagates along the v = axis we can write

$$E_m^{\parallel} = U_{\parallel} e^{-jk(m-\frac{1}{2}) d_1} , \tag{6}$$

$$E_m^{\perp} = U_{\perp} e^{-jk(m-\frac{1}{2}) d_1} . \tag{7}$$

We have solved Eqs (4) and (5) for the quantities

$$P_n^{\parallel} = \frac{e_n^{\parallel}}{U_{\parallel}} \exp \left[jk(m-\frac{1}{2}) d_1 - j\frac{\pi}{2} \right] , \tag{8}$$

$$P_n^{\perp} = \frac{e_n^{\perp}}{U_{\perp}} \exp \left[jk(m-\frac{1}{2}) d_1 - j\frac{\pi}{2} \right] \tag{9}$$

for the case when the rib depth T = 3 inches, its width d = 0.4 inches, ϵ = 4.1 and the frequency is 1.350 GHz. The results for $P_n^{\parallel}$ and $P_n^{\perp}$ are shown in Tables 1 and 2. Although we will not use them in this report we have also calculated $P_n^{'}$ and $P_n^{\perp}$ for a frequency of 3 GHz. These results are in Tables 3 and 4.

Table 1. Values of $P_n^{'}$ for T = 3.0", d = 0.4", ϵ = 4.1, N = 7, d_1 = 0.4286", and f = 1.35 GHz

n	$\lvert P_n^{'} \rvert$	Phase of $P_n^{'}$ (degrees)
1	0.9199	- 95.0
2	0.9578	-102.8
3	1.0398	-110.1
4	1.1651	-114.1
5	1.2929	-114.7
6	1.3873	-113.3
7	1.3945	-110.2

Table 2. Values of $P_n^{\perp}$ for T = 3.0", d = 0.4", ϵ = 4.1, N = 7, d_1 = 0.4286", and f = 1.35 GHz

n	$\mid P_n^{\perp} \mid$	Phase of $P_n^{\perp}$ (degrees)
1	0.3338	-84.5
2	0.2782	-89.2
3	0.2755	-89.4
4	0.2765	-92.9
5	0.2805	-94.2
6	0.2867	-95.3
7	0.3452	-99.0

Table 3. Values of $P_n^{\parallel}$ for T = 3", d = 0.4", ϵ = 4.1, d_1 = 0.4286", N = 7, and f = 3.0 GHz

n	$\mid P_n^{\parallel} \mid$	Phase of $P_n^{\parallel}$ (degrees)
1	1.0364	- 83.1
2	0.8293	-132.5
3	1.6219	-146.7
4	1.8056	-136.3
5	1.2758	-145.5
6	1.5761	-180.4
7	2.1850	-176.5

Table 4. Values of $P_n^{\perp}$ for T = 3", d = 0.4", ϵ = 4.1, d_1 = 0.4286", N = 7, and f = 3.0 GHz

n	$\mid P_n^{\perp} \mid$	Phase of $P_n^{\perp}$ (degrees)
1	0.3625	- 84.1
2	0.3392	- 95.1
3	0.3468	- 96.9
4	0.3400	- 97.5
5	0.3289	-101.8
6	0.3366	-106.3
7	0.4166	-114.6

Once the quantities $P_n^{\parallel}$ and $P_n^{\perp}$ are known it can be shown that the scattered electric field E_s is given by

$$\begin{bmatrix} E_s^{\parallel} \\ E_s^{\perp} \end{bmatrix} = C_1 H_0^{(2)}(k\rho_o) \sum_{n=1}^{N} \exp\left[-jk(n-\tfrac{1}{2}) d_1 (1-\cos\gamma)\right] \begin{bmatrix} P_n^{\parallel} & U_{\parallel} \\ P_n^{\perp} & U_{\perp}\cos\gamma \end{bmatrix} \quad (10)$$

where

$$C_1 \equiv \left(\frac{\pi ka}{2}\right)(\epsilon - 1) J_1(ka) .$$

Now the scattered electric field due to a current element I is

$$E_s = -\frac{\omega\mu_o}{4} H_0^{(2)}(k\rho_o) I . \quad (11)$$

Therefore upon equating Eqs (11) and (10) we can obtain the equivalent current which results in the scattered field E_s. We get

$$\begin{bmatrix} I_{\parallel} \\ I_{\perp} \end{bmatrix} = C_2 \sum_{n=1}^{N} \exp\left[-jk(n-\tfrac{1}{2}) d_1 (1-\cos\gamma)\right] \begin{bmatrix} P_n^{\parallel} & U_{\parallel} \\ P_n^{\perp} & U_{\perp}\cos\gamma \end{bmatrix} \quad (12)$$

where

$$C_2 = -2\pi a (\epsilon - 1) J_1(ka) \sqrt{\frac{\epsilon_o}{\mu_o}}$$

$$\simeq -\pi ka^2 (\epsilon - 1)\left(\frac{\epsilon_o}{\mu_o}\right)^{1/2} . \quad (13)$$

The last step in Eq. (13) follows because $ka \ll 1$. The equivalent surface current $J^s \equiv I/d$. Therefore upon using the definition $a^2 = d_1 d/\pi$ we get

$$\begin{bmatrix} J_{\parallel}^s \\ J_{\perp}^s \end{bmatrix} = C_3 \sum_{n=1}^{N} \exp\left\{-jk(n-\tfrac{1}{2}) d_1 (1-\cos\gamma)\right\} \begin{bmatrix} P_n^{\parallel} & U_{\parallel} \\ P_n^{\perp} & U_{\perp}\cos\gamma \end{bmatrix} \quad (14)$$

where

$$C_3 = -kd_1 (\epsilon - 1)\left(\frac{\epsilon_o}{\mu_o}\right)^{1/2} .$$

For small values of γ, Eq (14) takes the very simple form

$$\begin{bmatrix} J^s_{\parallel} \\ J^s_{\perp} \end{bmatrix} \simeq C_3 \sum_{n=1}^{N} \begin{bmatrix} P^{\parallel}_n & U_{\parallel} \\ P^{\perp}_n & U_{\perp} \end{bmatrix} . \tag{15}$$

We now must express the electric field components $U_{\parallel}$ and $U_{\perp}$ which are incident at the leading edge (v = 0) of the rib in terms of the fields on the reflector. If the rib is in the near zone of the aperture, it is reasonable to approximate the electric field at the rib by the electric field reflected by the dish. This is the negative of the electric field which is incident on the reflector from the feed horn. Therefore

$$\underline{U} = \underline{E}_{\text{reflected}} = -\underline{E}_{\text{incident}} = -\left(\frac{\mu_o}{\epsilon_o}\right)^{1/2} (\hat{n} \times \underline{H}_{\text{incident}}) , \tag{16}$$

where $H_{\text{incident}} = H_i$ is the quantity which appears in the integral in Eq (1). Therefore we can use Eq (16) in Eq (15) to write

$$\begin{bmatrix} J^s_{\parallel} \\ J^s_{\perp} \end{bmatrix} = kd_1 (\epsilon - 1) \sum_{n=1}^{N} \begin{bmatrix} P^{\parallel}_n & (\hat{n} \times \underline{H}_i)_{\parallel} \\ P^{\perp}_n & (\hat{n} \times \underline{H}_i)_{\perp} \end{bmatrix} . \tag{17}$$

Finally, upon realizing that Eq (1) represents the scattered field by a reflector with surface current $2(\hat{n} \times H_i)$ and using Eq (17) we can identify K as

$$\begin{bmatrix} K_{\parallel} \\ K_{\perp} \end{bmatrix} = \frac{kd_1 (\epsilon - 1)}{2} \sum_{n=1}^{N} \begin{bmatrix} P^{\parallel}_n \\ P^{\perp}_n \end{bmatrix} . \tag{18}$$

Now since the air-search reflector system is horizontally polarized, we therefore set

$$K = K_{\parallel} = \frac{kd_1 (\epsilon - 1)}{2} \sum_{n=1}^{N} P^{\parallel}_n \tag{19}$$

on the horizontal ribs and

$$K = \cos\theta_R K_{\parallel} + \sin\theta_R K_{\perp}$$

$$= \frac{kd_1}{2}(\epsilon - 1)\sum_{n=1}^{N}\left[0.53\,P_n^{\parallel} + 0.85\,P_n^{\perp}\right] \quad (20)$$

on the diagonal ribs in Figure 2.

Before closing this section, we should note that the quantities

$$K_{\parallel} = \frac{kd_1}{2}(\epsilon - 1)\sum_{n=1}^{N} P_n^{\parallel} \quad (21)$$

and

$$K_{\perp} = \frac{kd_1}{2}(\epsilon - 1)\sum_{n=1}^{N} P_n^{\perp} \quad (22)$$

are sometimes called[4] the induced current ratios for parallel and perpendicular polarization, respectively. The values calculated from Eqs (21), (22) and Tables 1 and 2 for $|K_{\parallel}|$ and $|K_{\perp}|$ are consistent with the results in Figures 38 and 39 in Chapter 5 of Ref 4.

3. RESULTS

By using the results derived in the previous sections, we have modified the computer program discussed in Parts 1 and 2 of this report, so as to include the effect of the radome. Figure 5 shows the effect of the radome on the element pattern of the reflector, that is, no multipath and secondary horn absent. The reader will note that, over the angles of interest (that is, $-10^{\circ} < \theta < 10^{\circ}$) for the studies done in Part 2, there is a negligible change in the radiation pattern. Using this new program, we have recomputed some of the results for altitude error presented in Part 2, and have found that for the L-band system there is no discernible change in the altitude error, that is, the altitude error plots with and without the radome are approximately the same.

4. Vidale, J.A. (1964) Microwave Scanning Antennas, R.C. Hansen, Ed., Academic Press, New York.

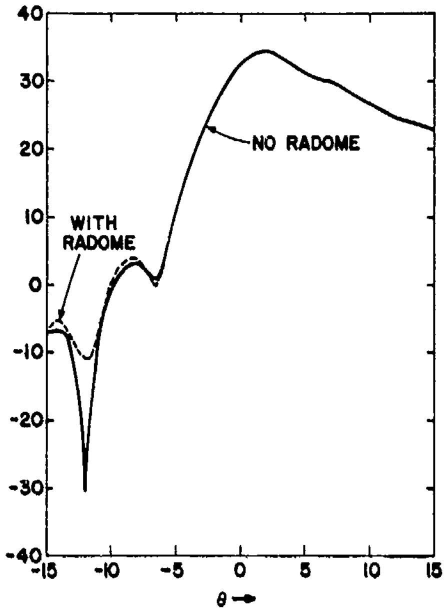

Figure 5. Effect of the Radome on the Radiation Pattern of the Air-Search Radar (L-band)

References

1. Blank, C. M. (1961) Effects of CW-396A Rigid Radome on AN FPS-6 Performance, Rome Air Development Center Report RADC-TN-61-189.
2. Kennedy, P. D. (1958) An Analysis of the Electrical Characteristics of Structurally Supported Radomes, Ohio State University, Antenna Laboratory Report 722-8.
3. Richmond, J. H. (1966) Scattering by a dielectric cylinder of arbitrary cross section shape, IEEE Trans. AP AP-14:334-341; 460-464.
4. Vidale, J. A. (1964) Microwave Scanning Antennas, R. C. Hansen, Ed., Academic Press, New York.

MISSION
of
Rome Air Development Center

RADC plans and conducts research, exploratory and advanced development programs in command, control, and communications (C^3) activities, and in the C^3 areas of information sciences and intelligence. The principal technical mission areas are communications, electromagnetic guidance and control, surveillance of ground and aerospace objects, intelligence data collection and handling, information system technology, ionospheric propagation, solid state sciences, microwave physics and electronic reliability, maintainability and compatibility.

AMERICAN REVOLUTION BICENTENNIAL 1776-1976

Printed by
United States Air Force
Hanscom AFB, Mass. 01731